



OPEN Preterm birth increases susceptibility to hyperglycemia induced glomerular alterations in male mice

Aleksandra Cwiek¹, Rachel K. Dailey², Ayyappa Kumar Sista Kameshwar³, Masako Suzuki³, Jaya Isaac⁴, Kimberly deRonde², Mark Conaway^{5,6}, Kevin M. Bennett⁷, Edwin J. Baldelomar⁷, Teng Li⁸, Teresa Wu⁸, Matthew R. Hoch⁹, Nicholas W. Chavkin^{10,11}, Patrick D. Walker¹², Karen K. Hirschi¹, Kimberly J. Reidy⁴ & Jennifer R. Charlton²✉

Diabetic kidney disease (DKD) is the leading cause of progressive chronic kidney disease in adults in the United States. However, the impact of preterm birth on the progression of DKD has not been studied. The goal of this project was to determine the effect of preterm birth on kidney health after exposure to hyperglycemia. CD-1 pups born preterm (19 days post conception (dpc)) and term (20 dpc) were studied, and outcomes of the male mice were reported. Preterm and term mice were treated with streptozotocin at six weeks to induce hyperglycemia. Body weight and blood sugar were monitored. Histologic, molecular, and imaging techniques were used to characterize the mice at 18 weeks. The preterm mice with diabetes had a lower podocyte density, lower proximal tubular fraction, and more atubular glomeruli compared to the term mice without diabetes. The preterm mice with diabetes also had a lower podocyte density and lower renin expression compared to term mice with diabetes. Based on single-cell RNA sequencing, the preterm mice with diabetes had increased expression of genes related to the angiogenesis migration pathway-related in endothelial cells and increased expression of genes in the actin adhesion pathway in podocytes compared to term mice with diabetes. Furthermore, the preterm mice with diabetes exhibited a weaker endothelial cell-podocyte interaction compared to term mice with diabetes. These data suggest that preterm birth increases susceptibility to glomerular and tubular damage after a brief “second hit” of hyperglycemia. In conclusion, preterm birth disrupts endothelial-podocyte crosstalk and increases susceptibility to kidney injury induced by hyperglycemia.

Keywords Diabetic kidney disease, Preterm birth, Streptozotocin, Chronic kidney disease, Endothelial-podocyte crosstalk, Cationic ferritin enhanced-MRI

Diabetic kidney disease (DKD) is the leading cause of chronic kidney disease (CKD) among adults in the United States¹. Diabetes currently affects 1 in 10 adults, and the number of individuals with or at risk for DKD continues to rise². DKD is characterized by podocyte loss that leads to increased urinary albumin excretion and kidney damage with reduced glomerular filtration rate³. DKD is also associated with increased mortality, adverse cardiovascular outcomes, and progression to advanced CKD. Despite therapeutic strategies aimed at controlling hyperglycemia, diabetes remains the leading cause of end stage kidney disease in adults. As new therapeutic approaches demonstrate remarkable promise in the prevention of CKD progression to end stage kidney disease,

¹Department of Cell Biology, University of Virginia School of Medicine, Charlottesville, VA, USA. ²Division of Nephrology, Department of Pediatrics, University of Virginia, Box 800386, Charlottesville, VA, USA. ³Department of Nutrition, Texas A&M University, College Station, TX, USA. ⁴Division of Nephrology, Department of Pediatrics, Children’s Hospital at Montefiore, New York, NY, USA. ⁵University of Virginia Health System, Charlottesville, VA, USA. ⁶Division of Translational Research and Applied Statistics, Department of Public Health Sciences, School of Medicine, University of Virginia, Charlottesville, VA, USA. ⁷Mallinckrodt Institute of Radiology, Washington University School of Medicine, St. Louis, MO, USA. ⁸School of Computing, Informatics, Decision Systems Engineering, Arizona State University, Tempe, AZ, USA. ⁹Department of Biomedical Engineering, University of Virginia, Charlottesville, VA, USA. ¹⁰Center for Developmental Biology and Regenerative Medicine, Seattle Children’s Research Institute, Seattle, WA, USA. ¹¹Department of Pediatrics, University of Washington School of Medicine, Seattle, WA, USA. ¹²Arkana Laboratories, Little Rock, AR, USA. ✉email: jrc6n@virginia.edu

it is critical to identify upstream risk factors for DKD in order to stratify individuals who may benefit from early interventions.

An early adverse maternal environment is strongly associated with adult kidney disease^{4–6}. Several studies have examined this relationship in rodent models of an adverse maternal environment by restricting protein during gestation. These studies have consistently found that rodents with a low birth weight had a low nephron number as adults^{7–11}. When these animals are exposed to diabetes as adults, glomerular alterations are commonly observed^{12,13}, suggesting that the adverse maternal environment is an upstream regulator of DKD.

Preterm birth is a form of adverse maternal environment, because the fetus is forced to continue organogenesis *ex utero*. Preterm birth is relatively common, occurring in approximately 10% of live births globally with 15 million infants born preterm each year¹⁴. Recently, preterm birth has been recognized as a general risk factor for CKD by international guidelines, including those from Kidney Disease Improving Global Outcomes (KDIGO)^{5,15–18}. Preterm birth has been associated with poor outcomes across a spectrum of kidney diseases, underscoring its significance as an upstream factor that influences long-term kidney health^{19–21}. Large epidemiological studies have demonstrated that individuals born preterm are at higher risk for developing both type 1 and type 2 diabetes^{22–24}. However, no clinical or preclinical studies have investigated whether preterm birth confers increased susceptibility to the development or progression of DKD.

The goal of this study was to characterize the early molecular, structural, and histopathological changes in mice born preterm after exposure to hyperglycemia and to determine which changes in mice exposed to hyperglycemia are attributable to preterm birth. To examine these early changes, we exposed mice born preterm to diabetes induced by streptozotocin. We hypothesized that the dual exposure of hyperglycemia and preterm birth would increase kidney damage compared to term mice with euglycemia. We further anticipated there would be structural alterations and dysregulation of gene expression in the kidneys of preterm mice exposed to hyperglycemia compared to term mice exposed to hyperglycemia, implicating preterm birth as an upstream risk factor in the development of DKD.

Methods and materials

Reagents and resources used in these experiments are shown in Supplementary Table 1.

Animals

Preterm mouse model

The Institutional Animal Care and Use Committee at the University of Virginia approved all the animal experiments. Experiments were performed in accordance with the National Institute of Health Guide for the Care and Use of Laboratory Animals and reported in accordance with ARRIVE (Animal Research: Reporting of In Vivo Experiments) guidelines. The outcomes of the male mice are reported here because there are known sex differences in diabetic nephropathy²⁵. By focusing on male mice, we were able to more clearly understand the effects of the experimental conditions rather than sex-specific variables. Timed pregnant CD-1 dams were purchased from Charles River Laboratory (Wilmington, MA, USA). CD-1 mice were used in this experiment as our previous work with other strains resulted in high perinatal mortality. Per Charles River protocol, dams were paired overnight with a male breeder. If a vaginal plug was observed the following morning, the female was considered pregnant (1 day post conception (dpc)). Pregnant mice were humanely euthanized via cervical dislocation using a previously published procedure²⁶, followed by Cesarean section (C/S) at 19 dpc. The offspring were removed from their amniotic sacs, and the placentas were manually separated from the pups. The pups were resuscitated in an incubator at 37 °C with 95% oxygen until their skin became pink and were placed with foster mothers that had recently delivered a litter via spontaneous vaginal birth. The foster mothers' pups were removed and humanely euthanized by carbon dioxide (CO₂) inhalation. Control animals were delivered vaginally at term (20 ± 0.25 dpc) and kept with their mothers. A previous study demonstrated no difference in mode of delivery between vaginal and C-section delivery²⁷. To reduce the risk of neglect and cannibalization in the preterm group, acepromazine maleate (Aceproject 10 mg/mL, final concentration: 75 mg/mL; Henry Schein Animal Health) was added to the water of the mothers 24 h prior to fostering and then for another 24 h. Mothers of the term pups did not receive this drug. Mice were housed according to institutional guidelines and weaned at three weeks. Body weights were recorded at weaning and then weekly. At six weeks, the mice were randomized to receive streptozotocin (STZ). At 18 weeks, the glomerular filtration rate (GFR) was measured, cationic ferritin was injected for imaging (see below), and the animals were euthanized. Tribromoethanol was administered via intraperitoneal (IP) injection to sedate the animal, followed by intracardiac perfusion with normal saline and then by 4% formalin. The kidneys were extracted, weighed, and prepared for histology, along with bulk and single-cell RNA sequencing, as outlined below.

Induction of hyperglycemia

At six weeks, the male offspring were assigned to one of the four cohorts: term nondiabetic (T-ND; *n* = 7), preterm nondiabetic (PT-ND; *n* = 6), term diabetic (T-D; *n* = 5), preterm diabetic (PT-D; *n* = 6). Following a four-hour fasting period, hyperglycemia was induced by streptozotocin (STZ, Zanosar Teva Pharmaceuticals, Irvine, CA) at 50 mg/kg IP per injection in five consecutive daily doses, as recommended by the Animal Models of Diabetic Complications Consortium protocol (see <https://www.diacomp.org/>). The low dose STZ protocol was also chosen because the high dose STZ protocol is associated with increased mortality. We chose to study our mice at 12 weeks after STZ as investigators²⁸ have shown mortality increases with this protocol as well in CD-1 mice 12 weeks after low dose STZ exposure. However at 12 weeks GFR remained normal and albuminuria was highly variable, supporting this as an early timepoint in the progression of DKD. The average blood glucose was previously 550 mg/dl at 21 days post exposure using this protocol²⁹. In the current study, plasma glucose levels were assessed prior to STZ injection at six weeks of age and again at one and six weeks after STZ exposure.

If the glucose level at six weeks was < 300 mg/dl, a second round of STZ injections in five consecutive daily doses were administered (T-D $n = 1$; PT-D $n = 2$).

Glomerular filtration rate

GFR was measured using a transcutaneous fluorescent detection device in the mice at 18 weeks of age (T-ND, $n = 4$; PT-ND, $n = 4$; T-D, $n = 3$; PT-D, $n = 5$). As previously published³⁰, an area on the back of each mouse was prepared; the fur was shaved, and a depilation cream was applied. A MediBeacon device (Mannheim, Germany) was attached using adhesive tape. Mice were injected with fluorescein isothiocyanate (FITC)-labeled sinistrin (7.5 mg/100 g BW) via the tail vein. The fluorescent signal of FITC-sinistrin was measured transcutaneously for 75–90 min at a sampling rate of 60 measurements/min and excitation time of 8 ms/measurement. Mice remained conscious and were monitored in individual cages while wearing the device. MPD Studio software (Mannheim Pharma and Diagnostics, Amtsgericht Mannheim, Germany) was used to create elimination kinetics curves and the GFR was calculated as previously reported³⁰.

Urine albumin to creatinine ratio

To assess for albuminuria, the urinary albumin to creatinine ratio (ACR) was calculated using a urine sample collected from the mice at 18 weeks of age and stored at -20 °C. The urinary ACR was quantified using the albumin detection kit Albuwell™ M (Mouse Albumin ELISA; Ethos Biosciences, Logan Township, NJ, USA) and DetectX® Urinary Creatinine Detection Kit (K002-H; Arbor Assays, Ann Arbor, MI, USA), according to the manufacturer's instructions.

Blood urea nitrogen

To assess blood urea nitrogen (BUN) levels, we used samples collected from the mice at the time of euthanasia at 18 weeks of age and stored at -20 °C. BUN was quantified using the DetectX® Urea Nitrogen (BUN) Colorimetric Detection Kit (Cat# K024-H1; Arbor Assays, Washtenaw County, MI, USA), according to the manufacturer's instructions.

Cationic ferritin enhanced-MRI

Cationic ferritin enhanced-MRI (CFE-MRI) was used to evaluate glomerular number (N_{glom}) and apparent glomerular size (aV_{glom}). Just before euthanasia, the mice were injected with horse spleen cationic ferritin (CF, 5.75 mg/100 g BW; F7879, Sigma Aldrich, St. Louis, MO) via two tail vein injections at 90 min intervals prior to euthanasia. The justification for this dose has been previously reported³⁰. Injections were followed by intracardiac perfusion with 0.9% saline and then with 4% formalin. Kidneys were imaged in PBS in customized container using 9.4 T MRI from Bruker (Billerica, MA). Images were acquired with a 3D gradient recalled echo (GRE) pulse sequence with a repetition time of 90 ms, echo time of 15 ms, field of view of 28 mm \times 42 mm \times 28 mm, matrix size of 512 \times 768 \times 512, flip angle 30°, and isotropic spatial resolution of 55 \times 55 \times 55 μm . The programs Fiji (<https://fiji.sc/>)³¹, 3D Slicer (<https://www.slicer.org/>)³², Matlab (The Mathworks, Natick, MA, <https://www.mathworks.com>), and Python (Python Software Foundation, <https://www.python.org/>) were used to segment the images and measure glomerular characteristics³⁰.

The raw images were imported into 3D Slicer, where each kidney was segmented using both the paintbrush tool and the 'fill between slices' tool to interpolate the segmentation across the kidney and medulla, providing two masks used to calculate kidney volume and cortical volume. Fiji was used to convert the images into the required PNG format for implementation of the UHDoG³³, a deep learning method based on Matlab and Python for glomerular segmentation. The glomerular number was determined from the segmentation masks using the connected components algorithm. The apparent size was estimated through the adjusted spherical model equation. Further methodological details have been previously published³⁴.

Stereologic evaluation of N_{glom}

To validate the CFE-MRI findings in this new model, we estimated N_{glom} using a previously published stereological technique^{35,36}. Glomeruli were segmented from PAS-stained sections ($n = 4/\text{animal}$) with a minimum distance of 100 μm between sections. This resulted in an average of 207 glomeruli per section and 807 glomeruli per animal. Using Amira software (Thermo Scientific), cortical area was determined by segmenting the entire kidney sample with subtraction of the areas of the medulla. Cortex and medulla were also manually segmented from slide images. All calculations were done using the established method³⁷.

Bulk RNA-sequencing analysis

Library preparation and sequencing

One kidney was stored in RNeasy Lysis Solution (Qiagen, Crawley, UK). RNA extraction and cleaning were performed using TRIzol (Invitrogen, Waltham, MA) and RNeasy MinElute Cleanup Kit with RNase-Free DNase (Qiagen, Hilden, Germany). Extracted RNA was reconstituted with RNase-free water to a final volume of 50 μl and stored at -80 °C until analysis. RNA concentration and OD260/280 were measured with a NanoDrop Spectrophotometer (Thermo Fisher, Waltham, MA). Whole kidney RNA-Seq was performed by Novogene, and only samples with high purity (OD260/280 > 2.0 ; RIN > 4.0) were analyzed. The detailed sequencing statistics are shown in Supplementary Table 2.

Data analysis

Sequencing quality was assessed using FastQC (<https://www.bioinformatics.babraham.ac.uk/projects/fastqc/>). Low-quality reads were discarded before the analyses. Obtained reads were adapter trimmed and then aligned to the GRCm38 mouse genome with the gencode M15 gene annotation using the STAR aligner³⁸. Transcripts were

quantified using the *--quantMode GeneCounts* function of the STAR aligner, and normalization was applied, followed by differential expression assessed using the DESeq2³⁹. Genes with mean normalized expression < 50 reads in all samples were filtered out because these are more likely to represent transcriptional noise. Differentially expressed genes (DEGs) with a p-value adjusted by false discovery rate (FDR) for multiple comparisons of < 0.05 and a fold change (FC) of at least 2 were selected to visualize and rank genes. The sequencing data that support the findings is available at GEO.

Single-cell RNA-sequencing analysis

Single cell sample preparation

The kidneys from four animals (one animal from each group: T-ND, T-D, PT-ND, and PT-D) were disassociated to isolate the cells for single cell RNA-Sequencing (scRNA-Seq). The kidneys were directly perfused via the left ventricle with 0.9% saline. The kidneys were rapidly dissected, moved to ice-cold PBS, then minced on ice using a scalpel. Each minced kidney was transferred into a 15 mL centrifuge tube with 2.0 mL of the protease solution for each half of the kidney (protease solution: ice-cold: 25 mM CaCl₂, 10 mg/mL B. Licheniformis protease, 125 U/mL DNase I, 1xDPBS). Samples were digested on ice and triturated using p1000 tip for 15 s every 2 min for a total of 20 min. The digestion was stopped by adding 3 mL of ice-cold PBS + 10% FBS and centrifuged at 1200 g for 5 min at 4 °C. The pellet was resuspended in 2 mL of PBS + 10% FBS, and cells were filtered through a 70-µm cell strainer and rinsed with 2 mL of PBS + 0.01% BSA. Next, cells were centrifuged and resuspended in 5 mL of PBS + 0.01% BSA. Cells were filtered the second time through a 40-µm cell strainer and rinsed with 2 mL of PBS + 0.01% BSA, centrifuged, and resuspended in 1 mL of 1x RBC Lysis Buffer. Red blood cell lysis was performed for 5 min with occasional shaking, at room temperature. The reaction was stopped by adding 20 mL of 1xPBS, cells were centrifuged at 1200 g for 5 min at 4 °C and resuspended in PBS + 0.04% BSA. Cell suspension was stained with Propidium Iodide (Thermo Fisher #P1304MP), and live cells were sorted using the BD FACSMelody cell sorter. Sorted cells were centrifuged at 1200 g for 5 min at 4 °C and resuspended in 50 µl of PBS + 0.04% BSA.

Library preparation and sequencing

Samples were processed and prepared for scRNA sequencing at University of Virginia, School of Medicine University of Virginia - UVA Genome Analysis and Technology Core (RRID: SCR_018883, 5P30 CA044579). Single-cell suspensions were introduced into a multi-channel microfluidics chip within the Chromium Controller (10x Genomics Inc., Pleasanton, CA, USA) to generate Gel Beads in Emulsion (GEMs), aiming for a cell recovery target of 5,000 cells. The single-cell suspension was processed using the 10x Genomics Chromium Single Cell System (10x Genomics, Inc.). Gene expression libraries were prepared with the Chromium™ Next GEM Single Cell 3' Kit v3.1, 16 rxns (PN-1000268), the Chromium™ Next GEM Chip G Single Cell Kit, 48 rxnt (PN-1000120), and the Chromium™ Dual Index Kit TT Set A 96 rxns (for 3' and 5' Gene Expression, TCR/BCR and Multiome) (PN- 1000215). A small portion of the prepared library was sequenced on the MiSeq to perform initial quality control, including checking cell count, assessing the quality of the library, and performing rapid cluster analysis, later the sequencing was performed on the NextSeq 500 sequencer. Raw sequence data were processed using Cell Ranger (10x Genomics, Inc) and Bcl2fastq (<https://support.illumina.com>), generating sample-specific FASTQ files. The fastq files were aligned to the mm10 (version 2020-A) reference transcriptome using the 'cell ranger count' function from Cell Ranger pipeline (v 7.0.1), resulting in a total of 17,326 cells estimated across all samples (3,727 cells in T-ND, 3,810 in PT-ND, 5,065 in T-D, and 4,742 in PT-D). The detailed sequencing statistics are shown in Supplementary Table 3. The sequencing data that support the findings is available at GEO.

Data analysis

The filtered gene barcode matrix files were further analyzed using Seurat (v 5.1.0). Genes detected in fewer than three cells and cells with fewer than 200 expressed genes were excluded from the analysis. Cells with mitochondrial gene expression exceeding 50% were deemed injured or apoptotic and were similarly excluded. A higher mitochondrial gene cutoff was used to account for the inherently elevated baseline mitochondrial content of the kidney and increased vulnerability to mitochondrial injury in proximal tubules associated with diabetic kidney disease⁴⁰. Also, parameters such as UMI counts per cell (nCount RNA), genes detected per cell (nFeature RNA) and low complex cells (log10GenesPerUMI > 0.80) were used to eliminate poor quality cells resulting in 17,374 genes across 9,247 cells. scTransform was used for performing normalization and variance stabilization to address technical variability and for effective integration of samples and downstream analysis. To build the K-nearest neighbor graph, the initial 30 principal components derived from principal-component analysis were included in FindNeighbor. Subsequently, we conducted an unsupervised clustering analysis using the Louvain algorithm, set to a resolution of 1.4, with the FindClusters followed by FindSubCluster with a resolution of 0.2. For dimensionality reduction and visualization, UMAP coordinates were computed with the RunUMAP, based on the same 30 principal components. Finally, cell type-specific marker genes were determined through FindAllMarkers, using the Wilcoxon rank-sum test for statistical significance. Differential gene expression analysis was performed between cells from groups using FindMarkers. Genes with avg Log2 fold change ≥ 2 (or) ≤ - 2 and multiple testing adjusted p-value ≤ 0.05 were considered significantly (up or down) regulated for further analysis. The gene ontology (GO) enrichment for the significantly differentially expressed genes was analyzed by clusterProfiler (v 4.12.1)⁴¹ and GO terms with p and q values ≤ 0.05 were considered significant. For enhanced visualization of UMAPs, clustered dot plots reported in this study were generated using scCustomize⁴².

Intercellular communication

CellChat (v2.1.2) was used to evaluate the cell-cell communications between the identified cell types. To identify conserved and specific signaling pathways, the annotated Seurat subset object of term diabetic (T-D) and preterm diabetic (PT-D) mice were used to create a CellChat object using the createCellChat function. CellChat is a curated database designed to study intercellular communication by integrating single-cell RNA sequencing (scRNA-Seq) data with its comprehensive database of ligand-receptor interactions, CellChatDB. This combination enables a systematic analysis of cell signaling dynamics and interactions across various cell types⁴³. Communication probabilities were calculated by incorporating gene expression data from each cell group, excluding intercellular communications when specific cell groups contained fewer than 10 cells. The differential interactions and their corresponding strengths among various cell types, including comparisons between T-D and PT-D groups, were systematically analyzed. The total number of interactions and the strength of interactions were compared across these groups, with changes in incoming and outgoing interaction strengths for each cell population visualized within a two-dimensional framework. Information flow, quantified as the aggregate communication probability between all cell population pairs within the inferred network, was assessed across different signaling pathways. By comparing these pathways, both conserved and disease-specific signaling pathways were identified, along with the associated up-regulated and down-regulated ligand-receptor pairs.

Histology and immunohistochemistry

A portion of formalin-fixed kidney tissue from each available animal was used for histological assessment. The kidneys were immersion-fixed in 10% buffered formalin for 24 h then embedded in paraffin. The kidneys were sectioned at a thickness of 5 μ m, deparaffinized with xylene, and rehydrated using ethanol in stepwise descending concentrations. To perform the atubular glomeruli assessment, the digital images of the whole kidney section were acquired using the Grundium Ocus with a 20x objective (© Grundium Ltd 2019). To measure the proximal tubular fractions, immunohistochemistry assessments were performed based on the images obtained using a Leica Microsystems CMS (Leica DM1000 LED) microscope and a DMC6200 digital camera.

PAS staining was performed to quantify pathology in the glomeruli, tubules, vasculature, or interstitial space. Slides were counterstained with Mayer's hematoxylin before the final wash. Pathologist (PW) reviewed the images. **Glomerular density:** Glomerular density was measured by the number of glomeruli divided by cortical area calculated using Amira software as previously published²⁶. **Proximal tubule fraction and atubular glomeruli:** In our previous published neonatal mouse study, several genes associated with the proximal tubule were identified in the preterm cohort. To determine whether these early changes resulted in pathology during adulthood, the proximal tubular fraction and the integrity of the junction between the glomerulus and tubule were evaluated. Tissue sections were subjected to enzymatic digestion with proteinase K, followed by biotinylated Lotus lectin stain (Vector Laboratories, Burlingame, CA, USA, B1325, 1:50 dilution). The sections were then washed with phosphate buffer and incubated in Vectastain ABC reagent3,3'-diaminobenzidine (DAB), followed by counterstaining with methylene blue solution before dehydration. Ten to fourteen additional images were captured from the subcapsular region, and the proximal tubular area was measured. Using the histogram tool in Amira software the "non-proximal tubule" area (including glomeruli, other sections of the tubule, interstitial space, and vasculature) was identified and labeled. This was subtracted from the total area of the section to give the proximal tubular area. The area of the proximal tubule was divided by the total area for proximal tubular fraction (Supplementary Fig. 2b). To identify disruption of the glomerulotubular junction, each glomerulus in the section was categorized as having lotus positive cells within or connecting to the glomerulus (Supplementary Fig. 2d). The number of lotus negative glomeruli divided by the total number of glomeruli were compared between the preterm and term groups as previously published^{26,44,45}. **Renin staining** was performed using an established protocol⁴⁶.

Podocyte density and glomerular area

Podocyte density and glomerular area were quantified using a protocol modified from Venkatareddy et al.⁴⁷ Dual IF Immunostaining for WT-1 (Santa Cruz, Rabbit, Anti-WT1, sc-192, 1:50 dilution) and synaptopodin (Acris Antibodies Mouse Anti-Synaptopodin, Clone G1D4, BM5086, 1:10 dilution) was performed using 5 μ m sections with sodium citrate retrieval and appropriate secondary antibodies (Jackson Immunoresearch). Hoechst was applied to stain nuclei (Supplementary Fig. 2a). Image J analytic software was used to quantify apparent mean WT + podocyte nuclear diameter and synaptopodin staining was used to quantify glomerular area. Podocyte density was calculated using the protocol described by Venkatareddy et al.⁴⁷ Approximately 10 glomeruli per kidney were selected for quantification in an unbiased fashion representing glomeruli throughout the 2D section. Investigators performing the quantification were blinded to the animal group.

Statistical analysis

Because the molecular analysis was the primary focus of this study and no preliminary data were available to calculate an effect size, a formal sample size calculation was not conducted. The Mann-Whitney nonparametric test for unpaired samples was used to analyze continuous variables between groups, with a $p < 0.05$ considered statistically significant. A one-sided t-test was used to compare T-D to PT-D groups. All graphs and analyses were generated using Prism 8.0 software (GraphPad).

Results

The experimental design is shown in (Fig. 1a). At six weeks of age, there was no difference in the body weights of any of the groups. By 15 weeks of age, both diabetic groups (T-D and PT-D) lost weight for the duration of the experimental period (Supplementary Fig. 1a). The kidney weights of preterm mice were not different from the term mice, but between the diabetic groups, the preterm kidneys (PT-D) weighed more than the term (T-D)

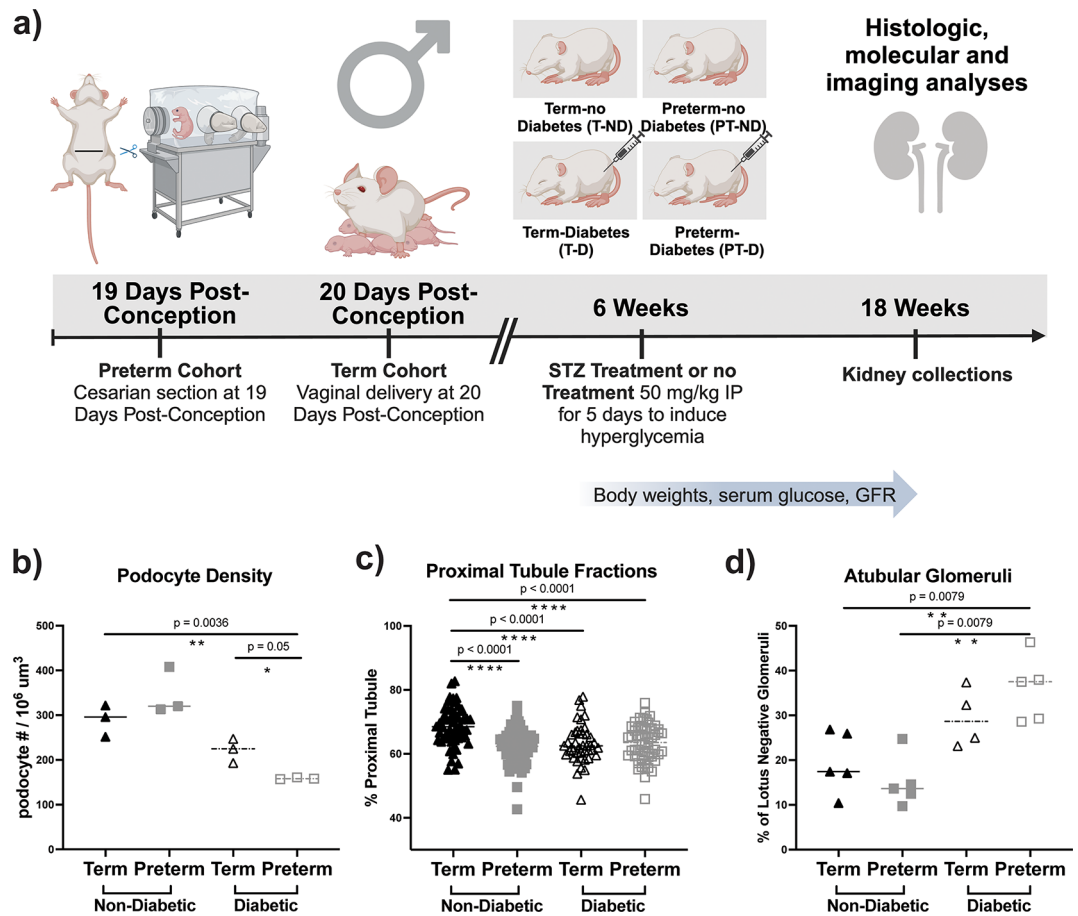


Fig. 1. Structural alterations in preterm mouse kidneys exposed to hyperglycemia. Preterm and term mice were exposed to STZ at six weeks of age and euthanized at 18 weeks of age (a). The preterm diabetic group (PT-D) had a lower podocyte density than the term non-diabetic group (T-ND) (b). Preterm nondiabetic, term diabetic and preterm diabetic groups had lower proximal tubule fractions than the term diabetic group. Each datapoint represents a measurement from one image. Ten to fourteen images were captured in the subcapsular region of each of the kidneys (c). Preterm diabetic mice had more atubular glomeruli than preterm non-diabetic and term non-diabetic mice (d). Mann Whitney test (b, c, d) with a p-value < 0.05 was considered statistically significant. A one-sided t-test was used to compare T-D to PT-D in b. Panel a was created in BioRender.com.

kidneys (Supplementary Fig. 1b). Three animals in the diabetic group (T-D, $n = 1$ and PT-D, $n = 2$) had a blood glucose concentration of < 300 mg/dl at six weeks post-injection and, therefore, received two injections of STZ. The average blood glucose of the T-D was 523 ± 109 mg/dl (T-ND: 130 ± 28 mg/dl) and PT-D was 535 ± 159 mg/dl (P-ND: 140 ± 42 mg/dl) (Supplementary Fig. 1c). There was no difference in GFR between any of the groups (Supplementary Fig. 1d). Although there was no statistical difference in urine albumin to creatinine ratio (urine ACR) between the groups, in both diabetic groups (T-D and PT-D) the mean ACR tended to be higher compared to their nondiabetic counterpart (T-ND and PT-ND, respectively) as an expected indicator of early diabetic nephropathy (Supplementary Fig. 1e). Serum urea nitrogen level (BUN) was higher in PT-D compared to T-ND and T-D, indicating early renal damage (Supplementary Fig. 1f).

Structural alterations in preterm mouse kidneys exposed to hyperglycemia (PT-D vs. T-ND)

We based our histologic assessment of these animals on previous work by our group²⁶ and others⁴⁸. There was no additive effect of hyperglycemia on glomerular density (Supplementary Fig. 1g). Podocyte density in the PT-D group was significantly lower than in the T-ND group (Fig. 1b).

We have previously reported early molecular changes in the proximal tubules²⁶ and studies have demonstrated hypertrophy of the proximal tubules in diabetic models⁴⁹. To evaluate the structure of the proximal tubules, we assessed the fraction of proximal tubules and the connection of the glomerulus to the tubule. Proximal tubule fractions were lower in PT-D group compared to the T-ND group (Fig. 1c, Supplementary Fig. 2c). The percentage of ATGs was significantly higher in the PT-D group compared to both the T-ND and PT-D (Fig. 1d).

Kidney volume, cortical volume, and glomerular number by CFE-MRI, were not different between the groups. There was no difference in glomerular number by CFE-MRI attributable to preterm birth in those with hyperglycemia (PT-D: 15,281 (IQR: 14,188 – 15,818 vs. T-D: 14,166 (IQR: 12,246 – 15,953)). There was also no

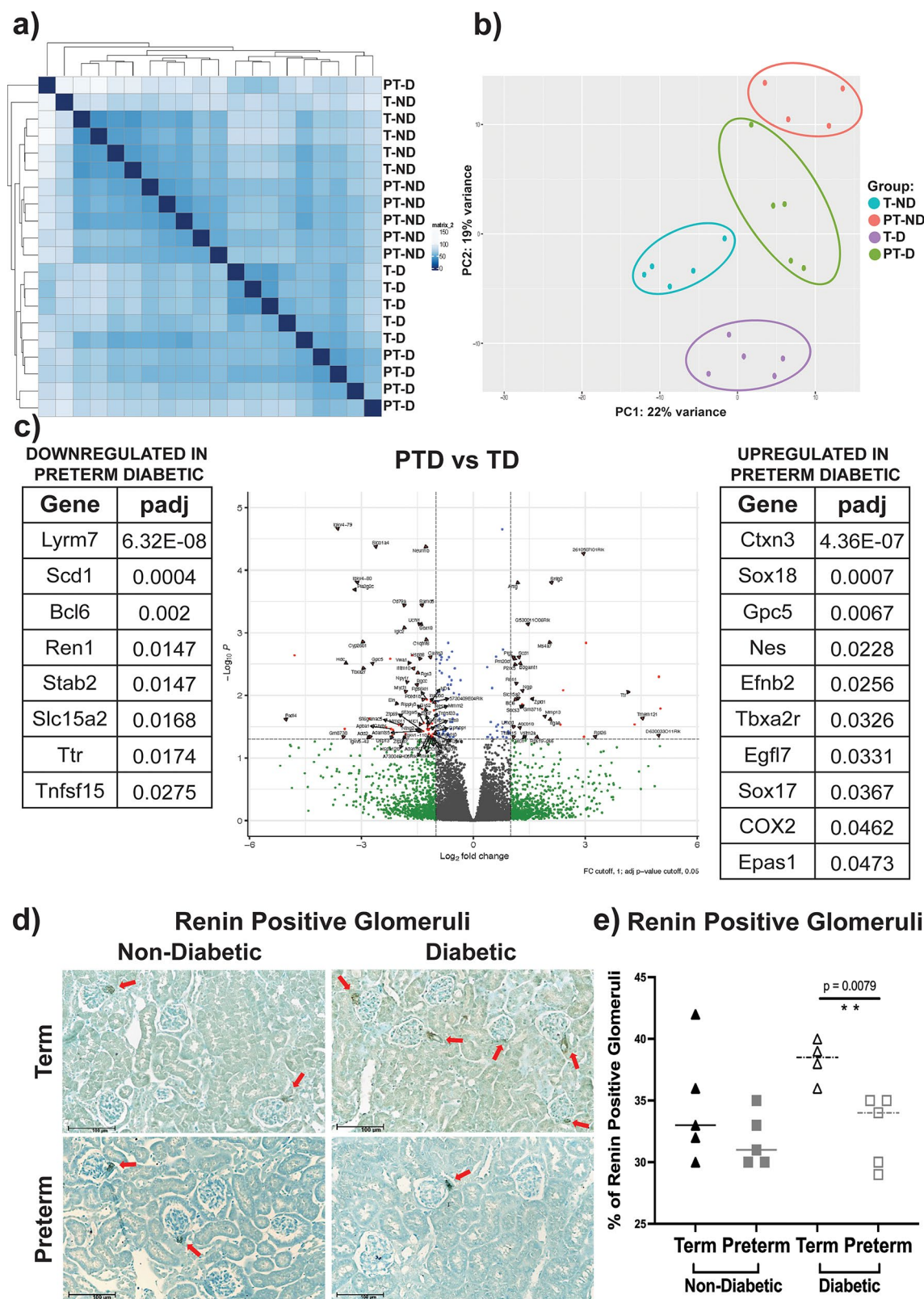


Fig. 2. Dual exposure to preterm birth and hyperglycemia results in transcriptional alterations in the kidney. Hierarchical clustering analysis of RNA-Seq data reveal the expression profiles clustering into four groups (a). A principal component analysis also showed clear dissociations between the expression profiles in all groups (b). Differentially expressed genes (DEGs) between preterm diabetic and term diabetic groups reveal differences in gene expression connected to the kidney vascularization, including renin (c). There were fewer renin positive glomeruli in the preterm diabetic group compared to term diabetic group (d, e).

difference in the PT-D compared to T-ND (P-TD: 15,281 (14,188 – 15,818) vs. T-D: 13,283 (13,077 – 15,035) groups (Supplementary Fig. 3a). There was no difference in the size of the glomeruli between the groups, although the variance in the PT-D group was large (Supplementary Fig. 3c, d). There was no difference in kidney volume or cortical volume by MRI between the groups (Supplementary Fig. 3e and f). Glomerular number by CFE-MRI and glomerular number obtained through stereology were similar, validating the CFE-MRI methodology for glomerular enumeration in this model (Supplementary Fig. 3a and b). Cationic ferritin successfully labeled the glomerular basement membrane of most of the kidneys from all four groups. In adequately labeled kidneys, glomeruli were detected as individual, punctuated dots on the MR images (Supplementary Fig. 3g). In some kidneys, the CF appeared in the lumen of the tubule resulting in inaccurate assessment of N_{glom} by CFE-MRI (MRI analysis included: T-ND: n=3; PT-ND: n=2; T-D: n=5; PT-D: n=3). Several of the diabetic animals also exhibited dilation of the ureter, consistent with osmotic diuresis.

Transcriptional alterations in preterm mouse kidneys exposed to hyperglycemia (PT-D vs. T-D)

Both bulk and single-cell RNA sequencing (RNA-Seq) were performed to identify molecular changes in the kidney attributable to preterm birth in the setting of hyperglycemia. From bulk RNA-Seq, an unsupervised analysis of the kidneys was performed. The expression profiles were clustered into four groups (with the exception of two samples), by hierarchical clustering (Fig. 2a). The PCA analysis revealed distinct clusters within the group, with the exception of one sample. Additionally, PC2, accounting for 19% of the variability, was correlated with the sample groups. T-ND and PT-D were the most distant among the groups (Fig. 2b). The groups with diabetes had distinct gene expression patterns compared to the groups without diabetes. The primary outcome for the gene expression analysis was the comparison of PT-D to the T-D. We identified 70 differentially expressed genes (DEGs) upregulated and 39 downregulated in PT-D compared to T-D (Fig. 2c). IHC for renin confirmed the findings identified on the gene expression analysis, showing fewer renin positive glomeruli in PT-D than in T-D (Fig. 2d and e). Bulk RNA-Seq also suggested abnormalities in the migration of blood vessel endothelial cells, evidenced by an upregulated GO term “negative regulation of blood vessel endothelial cell migration” in PT-D

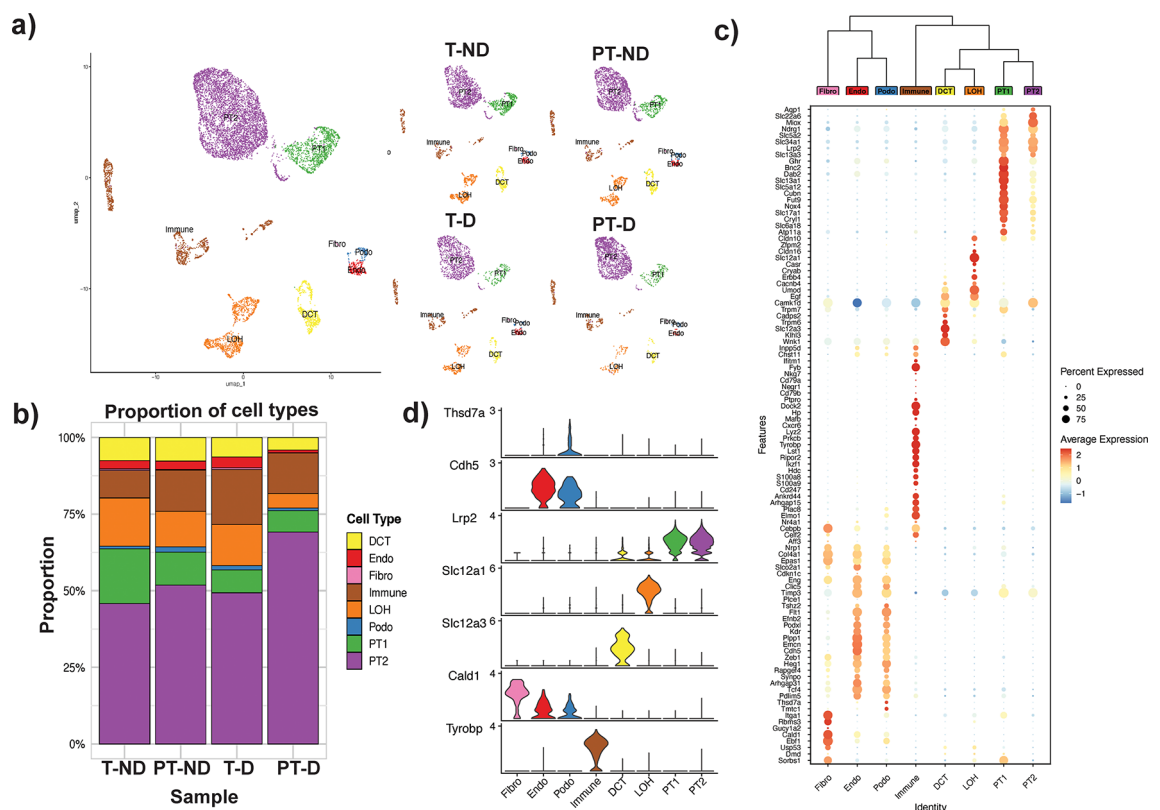


Fig. 3. Single-cell transcriptome profiles from hyperglycemic and control mouse kidneys. Single-cell profiles from the kidneys were integrated and cells clustered. Samples were integrated into one UMAP plot (a), and in one UMAP plot per condition (a). Cell sub-clusters summarized by general kidney cell type and relative cell proportions are indicated in one column per experimental group. DCT, Distal Convoluted Tubule; Endo, endothelial cell; Fibro, fibroblast; Immune, immune cell; LOH, Loop of Henle; Podo, Podocytes; PT1, Proximal Tubules type 1; PT2, Proximal Tubules Type 2 (b). (c) Average expression of key marker genes that were used to annotate specific cell clusters and sub-clusters (includes T-ND, T-D, PT-ND and PT-D). Stacked violin plot showing the expression of well-established gene markers (d).

compared to T-D (Supplementary Fig. 4a and c). GO enrichment analysis revealed that the electron transport-related genes were enriched in the genes that upregulated PT-D compared to T-D (Supplementary Fig. 4b and d).

Single-cell transcriptome profiles from the kidneys of the four experimental groups were integrated, resulting in 9,247 cells with 17,374 genes detected. Twenty-seven distinct clusters were identified (Fig. 3a). Cell types of each cluster were categorized using published cell type-specific marker genes (Fig. 3c) listed in Supplementary Table 4. Figure 3d shows the combined data from the control group (T-ND) and the three experimental conditions (T-D, PT-ND, PT-D). Phylogenetic analysis of cell identity classes using Seurat's BuildClusterTree algorithm revealed distinct hierarchical relationships: fibroblasts, endothelial cells, and podocytes formed one major clade, while distal convoluted tubule (DCT), loop of Henle (LOH), and proximal tubule (PT1 and PT2) cells constituted another. Immune cells formed a separate cluster, highlighting the diverse cellular composition of the tissue (Fig. 3c). Podocyte and endothelial specific genes were used to distinguish these cell clusters. Given that the experimental conditions could alter expression of these markers, the distinction between podocyte and endothelial cells was predominantly based on the T-ND sample (Supplemental Fig. 11). The proportions of cell clusters were summarized to compare their relative distributions among individual conditions (Fig. 3b). The PT-D group had a decreased proportion of endothelial cells compared to the T-D group (PT-D: 0.8% vs. T-D = 3.5%). The identified cell types and cell subsets were present in the diabetic and non-diabetic groups (Fig. 3a). Fibroblasts were not detected in the PT-ND group. Gene ontology (GO) enrichment analysis was performed to identify processes altered by preterm birth by comparing the PT-D and T-D groups. We focused this analysis on two cells of interest: endothelial cells and podocytes. The enriched Biological Processes GO terms are shown in Fig. 4a-d. Our single-cell pathway analysis in the endothelial cells revealed the upregulation of genes classified as modifiers of endothelial migration. This is consistent with our findings of decreased *Ren1* expression in bulk RNA-Seq and decreased expression of renin in the PT-D group. These findings suggest that preterm birth alters the endothelial cell response to hyperglycemia. The PT-D group demonstrated an upregulation of genes classified as modifiers of actin adhesion filaments in podocytes. This suggests that preterm birth alters the regulation of the actin cytoskeleton and cell matrix adhesion, both critical for the maintenance of podocyte health. Together, these dysregulated pathways in the PT-D suggest a mechanism for the decreased podocyte density observed in this cohort. Further analysis of these data using Molecular Function is included in Supplementary Figs. 5–8. CNET plots categorized by GO terms are also included in Supplementary Figs. 9 and 10.

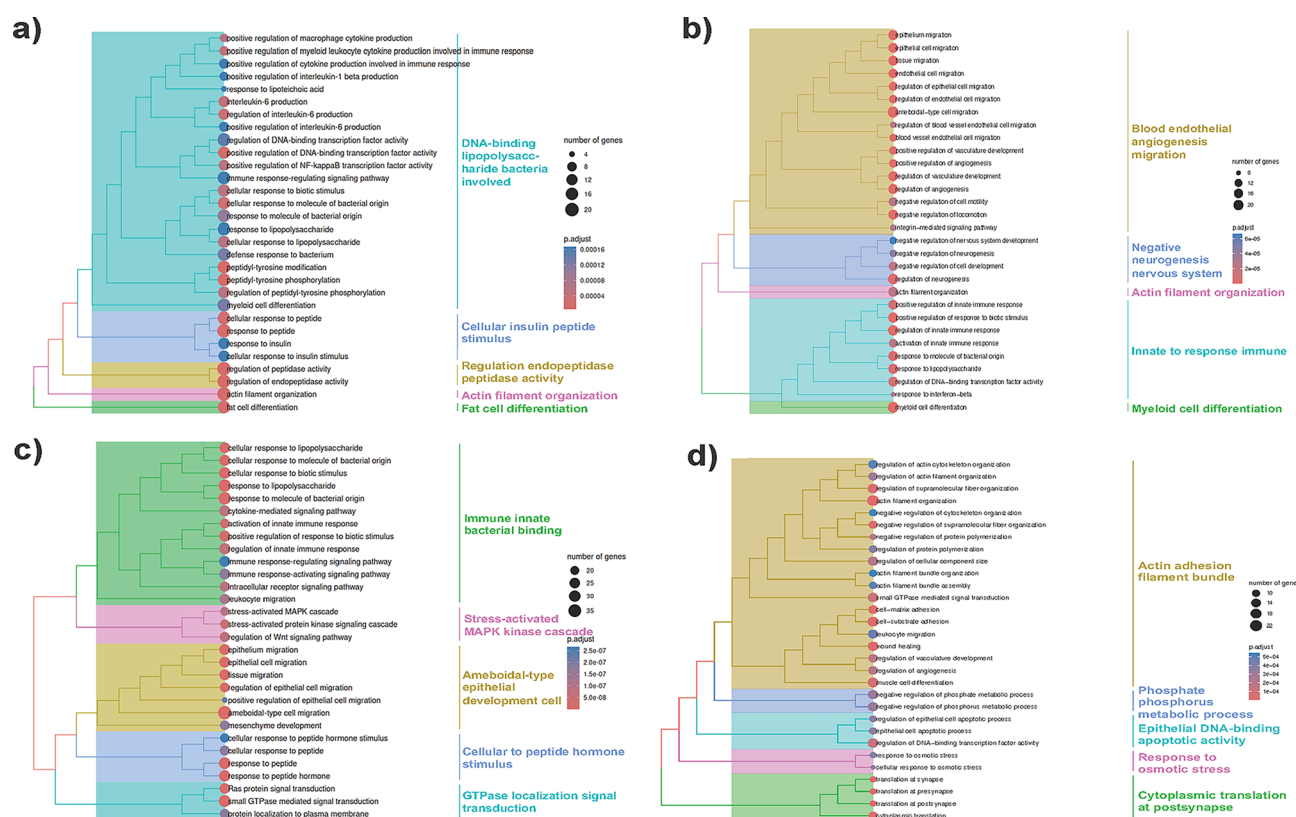


Fig. 4. Pathway changes in the endothelial cells and podocytes. **(a)** Genes upregulated in endothelial cells (ECs) of term diabetic and downregulated in preterm diabetic groups, with the Biological Processes as the GO term. **(b)** Genes downregulated in ECs of term diabetic and upregulated in preterm diabetic groups. GO term: Biological Processes. **(c)** Genes upregulated in podocytes of T-D and downregulated in PT-D. GO term: Biological Processes. **(d)** Genes downregulated in podocytes of T-D and upregulated in PT-D. GO term: Biological Processes.

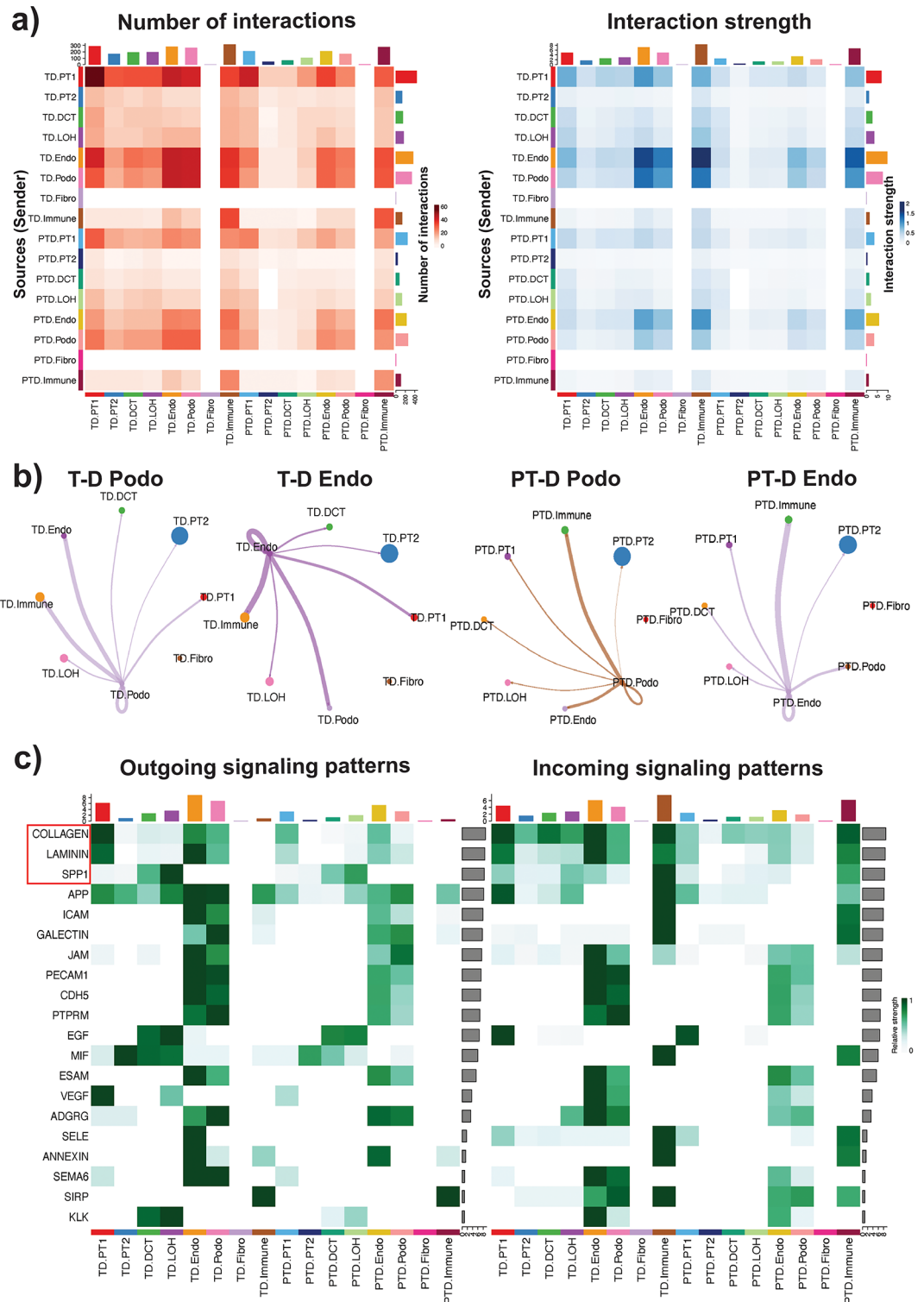


Fig. 5. Cellular communication analysis indicates weaker podocyte and endothelial cell interactions. Signaling interaction scores in term diabetic and preterm diabetic groups were evaluated by expression of ligand/receptor pairs in cells within the kidneys using CellChat. Heatmaps represent (left) the number of interactions and (right) interaction strength (adjusted according to cell number in the diabetic condition). (b) the circle plots represent cell-cell communication networks. The width of the edges indicates the strength of the communication. (c) The predicted outgoing and incoming signaling patterns in term diabetic and preterm diabetic groups and summarized as a heatmap. The color intensity represents differential interaction strength. Three most significant pathways are highlighted in the red box.

Cellular communication analysis indicates a weaker interaction between podocyte and endothelial cells in preterm mice with diabetes (PT-D vs. T-D)

Hyperglycemia was associated with perturbed gene expression across several cell types. To understand how these changes affect cell-cell communications, the cellular crosstalk based on the expression of known ligands and receptors was assessed. The number of interactions between selected cell types and the interaction strength (adjusted according to cell number) were determined by comparing the PT-D group to the T-D group (Fig. 5a). Significant reductions of cell-cell communication between endothelial cells and podocytes of PT-D compared (PT-D Endo and PT-D Podo) to T-D (T-D Endo and T-D Podo) were detected (Fig. 5b). Furthermore, mice with diabetes exhibited decreased outgoing and incoming signaling patterns across multiple crucial developmental and vascular pathways, including Collagen1, Laminin, and Spp1 (Fig. 5c, Supplementary Fig. 12). Within the T-D and PT-D groups the Collagen1 pathway was the one with the highest communication probability within this group with podocytes communicating with endothelial cells. Within the PT-D group, endothelial cells communicating with podocytes, there was an overall lower number of statistically significant communication probability pathway ligands (Supplementary Fig. 12).

Discussion

To our knowledge, this is the first study to evaluate the long-term effect of preterm birth on kidney structure and function in the setting of hyperglycemia. In this two “hit” model of early birth and adulthood exposure to hyperglycemia, the male preterm mice with diabetes had a lower podocyte density, decreased proximal tubular fraction, and more atubular glomeruli compared to the term mice without diabetes. Interestingly, no difference in nephron number was detected between the groups. Gene expression profiles and RNA sequencing analyses suggest that preterm birth in the setting of diabetes alters gene expression and cell-cell communication, particularly between the podocytes and endothelial cells. This study provides evidence that preterm birth increases the susceptibility of the podocyte and endothelial cells to the effects of hyperglycemia.

Diabetes has been shown to have a similar “second hit effect” on the kidney in other models of adverse maternal environments. Studies using maternal protein restriction as an adverse maternal environment also report decreased podocyte density, in addition to lower nephron number. Jones et al. reported that rat offspring exposed to low protein during gestation and then exposed to diabetes as adults had fewer nephrons, lower podocyte density and greater albuminuria compared to the normal protein mice with diabetes¹³. In a similar study, Gazzard et al. reported low protein mice exposed to diabetes also had fewer nephrons and developed a lower podocyte density with earlier onset albuminuria and histologic changes consistent with DKD than the normal protein mice with diabetes¹². These studies are consistent with our findings and demonstrate the importance of considering the upstream factors that interact with the second hit of diabetes to increase risk of CKD in individuals.

Several potential hypotheses have emerged to explain the association between preterm birth and CKD that parallel those seen in other settings of adverse maternal environments. The low nephron number^{50,51} and podocyte depletion⁵² hypotheses are the most cited and are also relevant in the setting of DKD progression^{12,13}. The nephron number hypothesis suggests that preterm infants are born with a lower nephron number and may not create as many nephrons as those born full term. Nearly 60% of a human's nephrogenesis occurs in gestational time frame of 28–36 weeks⁵³. Human and animal studies have shown that the window of nephrogenesis is likely shorter in those born preterm⁵⁴. Although human studies currently lack a direct measurement of nephron number in vivo, researchers have examined post-mortem kidney tissue from preterm neonates. These studies reveal fewer “layers” of glomeruli, indicating a potential reduction in the number of functional nephrons, and a higher percentage of morphologically abnormal glomeruli in preterm kidneys^{55,56}. In animal studies, mice born two days prior to full term gestation exhibited fewer glomeruli at young adulthood²⁷. Interestingly, there were no differences in the number of glomeruli in preterm group with or without diabetes. Several factors might explain the discrepancy between the published literature and this study. The preterm mice were born only one day early, in contrast to previous studies in which the mice were born two days early²⁷. Further, more atubular glomeruli were detected in the preterm and term diabetic mice than in the term nondiabetic mice. These data may imply that glomeruli exposed to hyperglycemia do not filter because they are disconnected from their tubules, while the glomeruli remain perfused.

The latter stages of diabetic nephropathy include podocyte injury, and podocyte loss may also contribute to poor kidney outcomes in the setting of diabetes after an adverse maternal environment, particularly in those born preterm. The predominant histologic finding in adolescents and adults born preterm is focal and segmental glomerulosclerosis (FSGS), a “podocytopathy”. Furthermore, preterm individuals who develop nephrotic syndrome, which primarily affects the podocytes, have worse outcomes, including faster decline of kidney function and decreased rate of complete remission, than their full-term counterparts^{19–21}. Biopsy data suggest that preterm birth can influence the number or function of the podocytes. In a single study of patients with FSGS, those born at an average gestational age of 25 weeks had 24% fewer podocytes than those born full term⁵⁷. Using a deconvolution technique on bulk RNA-Seq data, our group recently showed that mice born two days preterm, and studied just after birth, have a lower proportion of podocytes compared to full term mice²⁶.

In the milder preterm model in the current study, mice exposed to hyperglycemia were more susceptible to structural and molecular alternations in podocytes. We observe a lower podocyte density in the preterm mice with diabetes compared to the term mice with diabetes. Podocytes from the preterm mice with diabetes exhibited an increased stress response and an upregulation of actin adhesion filament bundles and alteration in collagen matrix signaling, suggesting that defective cell-cell and cell-matrix adhesion may have contributed to the loss of podocytes. Our data suggest that, independent of nephron number, preterm birth alters cell programming such that podocytes are more susceptible to the injury of hyperglycemia. This supports the podocyte depletion hypothesis by which preterm birth contributes to CKD progression.

Our model, demonstrating a lower podocyte density in the preterm mice with diabetes, is consistent with the literature suggesting podocytopathy in those born preterm. Early in life, preterm neonates appear to have over a 5-fold increase in the excretion of podocytes in their urine compared to full-term infants at matched, corrected gestational age⁵⁸. Studies of a preterm rat model have demonstrated a persistent, higher, and gradually accelerated podocyte depletion until 12 months (equivalent to middle adulthood in humans)⁴⁸. Kidney biopsy samples in humans have confirmed this finding⁵⁷. The podocyte depletion hypothesis suggests that progressive podocyte loss leads to proteinuria, glomerulosclerosis, and eventual end-stage kidney disease⁵⁹. Further longitudinal studies are needed to determine if this model develops glomerulosclerosis, a histologic finding associated with a low podocyte number.

In addition to the podocyte phenotype, several molecular alterations in the endothelial cells following exposure to hyperglycemia which are attributable to preterm birth were also identified. Clinical studies have demonstrated that preterm birth affects vasculogenesis in a wide array of developing organs^{60–62}. Indeed, we have previously reported changes in angiogenesis in this mouse preterm model just after birth²⁶, including fewer endothelial cells and a lower expression of genes that promote angiogenesis compared to full term mice. In the present work, further abnormalities in endothelial cell migration are suggested with changes in *Rgcc*, *Mmm2*, and *Tbxa2r*. The interaction between the podocytes and endothelial cells in preterm diabetic mice are weaker than in the diabetic term mice. These changes in cell-cell interactions may represent novel changes or an earlier onset of change that would develop with longer exposure to hyperglycemia in the term mice.

Interestingly, the expression of renin was lower in the kidneys of preterm diabetic mice compared to the term diabetic mice. Diabetes has generally been associated with circulating hyporeninemia, potentially due to juxtaglomerular injury or proximal tubular dysfunction, leading to decreased release of renin^{63,64}. Renal renin mRNA and renin within the juxtaglomerular apparatus and proximal tubule have also been shown to be lower in diabetic mice⁶⁴. In contrast, circulating renin levels in adolescents born preterm are similar to those born term, but alternate pathways within the renin angiotensin system may be affected⁶⁵. Our previous work has shown that *Ren1* expression was upregulated within the kidney in preterm mice at 27 dpc²⁶. Taken together, these data suggest that the effects of diabetes on the renin-angiotensin system may be more pronounced in those born preterm. Angiotensin converting enzyme (ACE) inhibition is the standard therapy for those with diabetic nephropathy, and our data suggest that more work is needed to understand the role of ACE inhibition in those born preterm with diabetes.

Limitations

There are several limitations of this study. In humans, nephrogenesis is typically complete at the time of full term, whereas in mice it continues for four days after birth. Our data suggest that a mouse born two days preterm is roughly equivalent in kidney development to a gestational age of 27 weeks in humans. Although this developmental disparity limits direct comparisons, our findings—along with those from previous studies—demonstrate that early delivery truncates nephrogenesis in mice²⁶ and leads to a CKD phenotype in early adulthood²⁷. These results parallel human autopsy studies⁵⁴ that indicate an early end to nephrogenesis in preterm neonates, and clinical observations of reduced kidney function in preterm infants²¹. Despite these inherent differences, the mouse model remains an important tool for dissecting CKD mechanisms that are challenging to investigate directly in humans.

This model represents a mild phenotype of both preterm birth and hyperglycemia. STZ-induction of hyperglycemia is well recognized as a variable model and hyperglycemia may not be induced with a single injection of STZ. We included several animals that required two injections of STZ, recognizing that these mice had a shorter total exposure to hyperglycemia. The STZ model primarily represents type 1 diabetes, which accounts for only about 10% of diabetic cases. However, individuals born preterm are at increased risk for both type 1 and type 2 diabetes²². Given that beta cell development largely occurs in late gestation, there is the possibility that diabetes in those born preterm may be related to less insulin production with more of a type 1 phenotype, in addition to insulin resistance. While type 2 diabetes models could offer additional insight, many rely on genetic approaches constrained by the CD-1 background required for the preterm model.

Finally, our single cell analysis did not have a significant expression of *Nphs1* or *Nphs2* to use these genes to identify podocytes. Because this project was designed to study all the cell types of the kidney, we did not enrich for podocytes or endothelial cells and as a result had a low yield of these rarer types of cells, consistent with other publications⁶⁶. Due to the small sample size of the cell populations, future studies should include enrichment of glomerular cells.

In conclusion, preterm birth is an early primary risk factor that is likely to exacerbate DKD progression. With the major advances in neonatal health care, the gestational age of viability is 22 weeks' gestation, and a majority of preterm infants survive into adulthood. As a result, clinicians will increasingly encounter adult patients with diabetes who were born preterm. At the same time, new drug therapies have been developed that could reduce or eliminate the progression of CKD in individuals who are at risk. This work provides evidence that preterm birth is an upstream risk factor for kidney disease in those who develop diabetes. Individuals born preterm who become diabetic may require more focused care, including risk stratification based on preterm birth in clinical trials, and possibly earlier interventions for those born preterm to prevent progression of DKD.

Data availability

Sequence data that support the findings of this study have been deposited in the GEO with the primary accession code: GSE280782.

Received: 16 October 2024; Accepted: 24 April 2025

Published online: 29 May 2025

References

1. Prevention, C. f. D. C. A. (Atlanta (GA: US Department of Health and Human Services, Centers for Disease Control and Prevention, 2021).
2. WHO. *Diabetes*, (2024). <https://www.who.int/news-room/fact-sheets/detail/diabetes>
3. Østerby, R. et al. A strong correlation between glomerular filtration rate and filtration surface in diabetic nephropathy. *Diabetologia* **31**, 265–270. <https://doi.org/10.1007/bf00277406> (1988).
4. Hoy, W. E., Rees, M., Kile, E., Mathews, J. D. & Wang, Z. A new dimension to the Barker hypothesis: low birthweight and susceptibility to renal disease. *Kidney Int.* **56**, 1072–1077. <https://doi.org/10.1046/j.1523-1755.1999.00633.x> (1999).
5. White, S. L. et al. Is low birth weight an antecedent of CKD in later life?? A systematic review of observational studies. *Am. J. Kidney Dis.* **54**, 248–261. <https://doi.org/10.1053/j.ajkd.2008.12.042> (2009).
6. Vikse, B. E., Irgens, L. M., Leivestad, T., Hallan, S. & Iversen, B. M. Low birth weight increases risk for end-stage renal disease. *J. Am. Soc. Nephrol.* **19**, 151–157. <https://doi.org/10.1681/ASN.2007020252> (2008).
7. Hoppe, C. C., Evans, R. G., Bertram, J. F. & Moritz, K. M. Effects of dietary protein restriction on nephron number in the mouse. *Am. J. Physiol. Regul. Integr. Comp. Physiol.* **292**, R1768–1774. <https://doi.org/10.1152/ajpregu.00442.2006> (2007).
8. Hoppe, C. C. et al. Combined prenatal and postnatal protein restriction influences adult kidney structure, function, and arterial pressure. *Am. J. Physiol. Regul. Integr. Comp. Physiol.* **292**, R462–469. <https://doi.org/10.1152/ajpregu.00079.2006> (2007).
9. Langley-Evans, S. C. Developmental programming of health and disease. *Proceedings of the Nutrition Society* **65**, 97–105 (2006). <https://doi.org/10.1079/pns2005478>
10. Gray, S. P., Denton, K. M., Cullen-McEwen, L., Bertram, J. F. & Moritz, K. M. Prenatal exposure to alcohol reduces nephron number and raises blood pressure in progeny. *J. Am. Soc. Nephrol.* **21**, 1891–1902. <https://doi.org/10.1681/ASN.2010040368> (2010).
11. Singh, R. R. et al. Prenatal corticosterone exposure results in altered AT1/AT2, nephron deficit and hypertension in the rat offspring. *J. Physiol.* **579**, 503–513. <https://doi.org/10.1113/jphysiol.2006.125773> (2007).
12. Gazzard, S. E., Van Der Wolde, J., Haruhara, K. & Bertram, J. F. Cullen-McEwen, L. A. Nephron deficit and low podocyte density increase risk of albuminuria and glomerulosclerosis in a model of diabetes. *Physiological Rep.* **11** <https://doi.org/10.14814/phy2.15579> (2023).
13. Jones, S. E., White, K. E., Flyvbjerg, A. & Marshall, S. M. The effect of intrauterine environment and low glomerular number on the histological changes in diabetic glomerulosclerosis. *Diabetologia* **49**, 191–199. <https://doi.org/10.1007/s00125-005-0052-z> (2006).
14. March of Dimes Prematurity Profile, <https://www.marchofdimess.org/peristats/reports/united-states/prematurity-profile> (.).
15. Stevens, P. E. et al. KDIGO 2024 clinical practice guideline for the evaluation and management of chronic kidney disease. *Kidney Int.* **105**, S117–S314. <https://doi.org/10.1016/j.kint.2023.10.018> (2024).
16. Ruggajo, P. et al. Low birth weight and risk of progression to end stage renal disease in IgA Nephropathy—A retrospective Registry-Based cohort study. *PLOS ONE*. **11**, e0153819. <https://doi.org/10.1371/journal.pone.0153819> (2016).
17. Crump, C., Sundquist, J., Winkleby, M. A. & Sundquist, K. Preterm birth and risk of chronic kidney disease from childhood into mid-adulthood: National cohort study. *BMJ* **365**, l1346. <https://doi.org/10.1136/bmj.l1346> (2019).
18. Hsu, C. W., Yamamoto, K. T., Henry, R. K., De Roos, A. J. & Flynn, J. T. Prenatal risk factors for childhood CKD. *J. Am. Soc. Nephrol.* **25**, 2105–2111. <https://doi.org/10.1681/asn.2013060582> (2014).
19. Isaac, J. S. et al. Association of preterm birth with adverse glomerular disease outcomes in children and adults. *Clin. J. Am. Soc. Nephrol.* <https://doi.org/10.2215/CJN.0000000000000475> (2024).
20. Chen, C. C., Yu, T., Chou, H. H., Chiou, Y. Y. & Kuo, P. L. Premature birth carries a higher risk of nephrotic syndrome: a cohort study. *Sci. Rep.* **11**, 20639. <https://doi.org/10.1038/s41598-021-00164-2> (2021).
21. Hingorani, S. et al. The association of low birthweight and prematurity on outcomes in children and adults with nephrotic syndrome—a NEPTUNE cohort study. *Pediatr. Nephrol.* **38**, 3297–3308. <https://doi.org/10.1007/s00467-023-05876-3> (2023).
22. Crump, C., Sundquist, J. & Sundquist, K. Preterm birth and risk of type 1 and type 2 diabetes: a National cohort study. *Diabetologia* **63**, 508–518. <https://doi.org/10.1007/s00125-019-05044-z> (2020).
23. Dinerstein, A. et al. Presence of metabolic syndrome markers in very low birth weight ex-premature infants during early adolescence. *J. Pediatr. Endocrinol. Metab.* **37**, 613–621. <https://doi.org/10.1515/jpem-2023-0308> (2024).
24. Holman-Vittone, A. et al. Associations of maternal preterm birth with subsequent risk for type 2 diabetes in women from the women's health initiative. *J. Dev. Origins Health Disease.* **14**, 333–340. <https://doi.org/10.1017/s2040174423000089> (2023).
25. Clotet-Freixas, S. et al. Sex differences in kidney metabolism May reflect sex-dependent outcomes in human diabetic kidney disease. *Sci. Transl. Med.* **16**, eabm2090. <https://doi.org/10.1126/scitranslmed.abm2090> (2024).
26. Cwiek, A. et al. Premature differentiation of nephron progenitor cell and dysregulation of gene pathways critical to kidney development in a model of preterm birth. *Sci. Rep.* **11**, 21667. <https://doi.org/10.1038/s41598-021-00489-y> (2021).
27. Stelloh, C. et al. Prematurity in mice leads to reduction in nephron number, hypertension, and proteinuria. *Transl Res.* **159**, 80–89. <https://doi.org/10.1016/j.trsl.2011.10.004> (2012).
28. Harris, R. & C. An outbred mouse strain to study diabetic nephropathy. &. (Vanderbilt University School, (2009).
29. Furman, B. L. Streptozotocin-Induced diabetic models in mice and rats. *Curr. Protocols.* **1** <https://doi.org/10.1002/cpz1.78> (2021).
30. Charlton, J. R. et al. Magnetic resonance imaging accurately tracks kidney pathology and heterogeneity in the transition from acute kidney injury to chronic kidney disease. *Kidney Int.* **99**, 173–185. <https://doi.org/10.1016/j.kint.2020.08.021> (2021).
31. Schindelin, J. et al. Fiji: an open-source platform for biological-image analysis. *Nat. Methods.* **9**, 676–682. <https://doi.org/10.1038/nmeth.2019> (2012).
32. Fedorov, A. et al. 3D slicer as an image computing platform for the quantitative imaging network. *Magn. Reson. Imaging.* **30**, 1323–1341. <https://doi.org/10.1016/j.mri.2012.05.001> (2012).
33. Xu, Y., Wu, T., Gao, F., Charlton, J. R. & Bennett, K. M. Improved small blob detection in 3D images using jointly constrained deep learning and Hessian analysis. *Sci. Rep.* **10** <https://doi.org/10.1038/s41598-019-57223-y> (2020).
34. Baldelomar, E. J., Charlton, J. R., Beeman, S. C. & Bennett, K. M. Measuring rat kidney glomerular number and size in vivo with MRI. *Am. J. Physiol. Ren. Physiol.* **314**, F399–F406. <https://doi.org/10.1152/ajprenal.00399.2017> (2018).
35. Baldelomar, E. J. et al. Phenotyping by magnetic resonance imaging nondestructively measures glomerular number and volume distribution in mice with and without nephron reduction. *Kidney Int.* **89**, 498–505. <https://doi.org/10.1038/ki.2015.316> (2016).
36. WEIBEL, E. R. & GOMEZ, D. M. A principle for counting tissue structures on random sections. *J. Appl. Physiol.* **17**, 343–348. <https://doi.org/10.1152/jappl.1962.17.2.343> (1962).
37. Baldelomar, E. J. et al. Mapping nephron mass in vivo using positron emission tomography. *Am. J. Physiol. Ren. Physiol.* **320**, F183–F192. <https://doi.org/10.1152/ajprenal.00418.2020> (2021).
38. Dobin, A. et al. STAR: ultrafast universal RNA-seq aligner. *Bioinformatics* **29**, 15–21. <https://doi.org/10.1093/bioinformatics/bts635> (2013).
39. Love, M. I., Huber, W. & Anders, S. Moderated Estimation of fold change and dispersion for RNA-seq data with DESeq2. *Genome Biol.* **15** <https://doi.org/10.1186/s13059-014-0550-8> (2014).
40. Park, J. et al. Single-cell transcriptomics of the mouse kidney reveals potential cellular targets of kidney disease. *Science* **360**, 758–763. <https://doi.org/10.1126/science.aar2131> (2018).

41. Wu, T. et al. ClusterProfiler 4.0: A universal enrichment tool for interpreting omics data. *Innov.* **2**, 100141. <https://doi.org/10.1016/j.xinn.2021.100141> (2021).
42. Samuel, M. (ed) Maëlle Salmon (Zenodo, (2021).
43. Jin, S. et al. Inference and analysis of cell-cell communication using cellchat. *Nat. Commun.* **12** <https://doi.org/10.1038/s41467-021-21246-9> (2021).
44. Charlton, J. R. et al. Beyond the tubule: pathogenic variants in LRP2, encoding the Megalin receptor, result in glomerular loss and early progressive chronic kidney disease. *Am. J. Physiol. Ren. Physiol.* <https://doi.org/10.1152/ajprenal.00295.2020> (2020).
45. Galarreta, C. I. et al. Tubular obstruction leads to progressive proximal tubular injury and atubular glomeruli in polycystic kidney disease. *Am. J. Pathol.* **184**, 1957–1966. <https://doi.org/10.1016/j.ajpath.2014.03.007> (2014).
46. Belyea, B. C. et al. Overexpression of Notch signaling in Renin cells leads to a polycystic kidney phenotype. *Clin. Sci. (Lond)*. **137**, 35–45. <https://doi.org/10.1042/CS20220496> (2023).
47. Venkatreddy, M. et al. Estimating podocyte number and density using a single histologic section. *J. Am. Soc. Nephrol.* **25**, 1118–1129. <https://doi.org/10.1681/ASN.2013080859> (2014).
48. Zhang, L. et al. Preterm birth leads to a decreased number of differentiated podocytes and accelerated podocyte differentiation. *Front. Cell. Dev. Biology.* **11** <https://doi.org/10.3389/fcell.2023.1142929> (2023).
49. Kawaguchi, T. et al. Diabetic condition induces hypertrophy and vacuolization in glomerular parietal epithelial cells. *Sci. Rep.* **11** <https://doi.org/10.1038/s41598-021-81027-8> (2021).
50. Brenner, B. M. & Chertow, G. M. Congenital oligonephropathy and the etiology of adult hypertension and progressive renal injury. *Am. J. Kidney Dis.* **23**, 171–175 (1994).
51. Brenner, B. M. & Chertow, G. M. Congenital oligonephropathy: an inborn cause of adult hypertension and progressive renal injury? *Curr. Opin. Nephrol. Hypertens.* **2**, 691–695 (1993).
52. Wiggins, R. C. The spectrum of podocytopathies: A unifying view of glomerular diseases. *Kidney Int.* **71**, 1205–1214. <https://doi.org/10.1038/sj.ki.5002222> (2007).
53. Hinchliffe, S. A., Sargent, P. H., Howard, C. V., Chan, Y. F. & van Velzen, D. Human intrauterine renal growth expressed in absolute number of glomeruli assessed by the disector method and Cavalieri principle. *Lab. Invest.* **64**, 777–784 (1991).
54. Carpenter, J., Yarlagaadda, S., Vandenheuvel, K. A., Ding, L. & Schuh, M. P. Human nephrogenesis can persist beyond 40 postnatal days in preterm infants. *Kidney Int. Rep.* **9**, 436–450. <https://doi.org/10.1016/j.ekir.2023.10.032> (2024).
55. Ryan, D. et al. Development of the human fetal kidney from mid to late gestation in male and female infants. *EBioMedicine* **27**, 275–283. <https://doi.org/10.1016/j.ebiom.2017.12.016> (2018).
56. Sutherland, M. R. et al. Accelerated maturation and abnormal morphology in the preterm neonatal kidney. *J. Am. Soc. Nephrol.* **22**, 1365–1374. <https://doi.org/10.1681/asn.2010121266> (2011).
57. Ikezumi, Y. et al. Low birthweight and premature birth are risk factors for podocytopenia and focal segmental glomerulosclerosis. *Am. J. Nephrol.* **38**, 149–157. <https://doi.org/10.1159/000353898> (2013).
58. Kent, A. L., Brown, L., Broom, M., Broomfield, A. & Dahlstrom, J. E. Increased urinary podocytes following indomethacin suggests drug-induced glomerular injury. *Pediatr. Nephrol.* **27**, 1111–1117. <https://doi.org/10.1007/s00467-012-2111-2> (2012).
59. Puelles, V. G. et al. mTOR-mediated podocyte hypertrophy regulates glomerular integrity in mice and humans. *JCI Insight.* **4** <https://doi.org/10.1172/jci.insight.99271> (2019).
60. Sixtus, R. P., Dyson, R. M. & Gray, C. L. Impact of prematurity on lifelong cardiovascular health: structural and functional considerations. *Npj Cardiovasc. Health.* **1** <https://doi.org/10.1038/s44325-024-00002-0> (2024).
61. Sutherland, M. R. et al. Preterm birth and hypertension risk. *Hypertension* **63**, 12–18. <https://doi.org/10.1161/hypertensionaha.113.01276> (2014).
62. Pravia, C. I. & Benny, M. Long-term consequences of prematurity. *Cleve. Clin. J. Med.* **87**, 759–767. <https://doi.org/10.3949/ccjm.87a.19108> (2020).
63. Massolini, B. D. et al. Therapeutic Renin Inhibition in diabetic Nephropathy—A review of the physiological evidence. *Front. Physiol.* **11** <https://doi.org/10.3389/fphys.2020.00190> (2020).
64. Tang, J. et al. Urinary Renin in patients and mice with diabetic kidney disease. *Hypertension* **74**, 83–94. <https://doi.org/10.1161/hypertensionaha.119.12873> (2019).
65. South, A. M. et al. Association between preterm birth and the renin – angiotensin system in adolescence. *J. Hypertens.* **36**, 2092–2101. <https://doi.org/10.1097/hjh.0000000000001801> (2018).
66. Wu, H., Kirita, Y., Donnelly, E. L. & Humphreys, B. D. Advantages of Single-Nucleus over Single-Cell RNA sequencing of adult kidney: rare cell types and novel cell States revealed in fibrosis. *J. Am. Soc. Nephrol.* **30**, 23–32. <https://doi.org/10.1681/ASN.2018090912> (2019).

Author contributions

J.R.C., A.C., K.d.R. planned and carried out the experiments. R.K.D, A.K.S, M.S. and M.C. performed the data analysis and all authors contributed to the interpretation of the results. A.C., M.S., K.J.R. and J.R.C. wrote the first draft of the manuscript. All authors provided critical feedback and helped shape the research and analysis. All authors reviewed and approved the final manuscript.

Funding

JRC, MS, KJR: R01HD111052, JRC (direct): U24DK115255-04, JRC (indirect): P50DK096373-11, R21DK134104-01, UVA Genome Analysis and Technology Core: RRID: SCR_018883, 5P30 CA044579, Imaging data were acquired through the University of Virginia Molecular Imaging Core Laboratory with National Institutes of Health S10OD025024 funding.

Declarations

Competing interests

The authors declare no competing interests.

Disclosures

JRC: VP of NKC; owner of Sindri Technologies LLC, investor in ZorroFlow and consultant for Mozarc Medical; KMB: Co-owner of Sindri Technologies LLC, Co-owner of XN Biotechnologies LLC; EJB: Co-owner of XN Biotechnologies LLC.

Additional information

Supplementary Information The online version contains supplementary material available at <https://doi.org/10.1038/s41598-025-00103-5>.

Correspondence and requests for materials should be addressed to J.R.C.

Reprints and permissions information is available at www.nature.com/reprints.

Publisher's note Springer Nature remains neutral with regard to jurisdictional claims in published maps and institutional affiliations.

Open Access This article is licensed under a Creative Commons Attribution-NonCommercial-NoDerivatives 4.0 International License, which permits any non-commercial use, sharing, distribution and reproduction in any medium or format, as long as you give appropriate credit to the original author(s) and the source, provide a link to the Creative Commons licence, and indicate if you modified the licensed material. You do not have permission under this licence to share adapted material derived from this article or parts of it. The images or other third party material in this article are included in the article's Creative Commons licence, unless indicated otherwise in a credit line to the material. If material is not included in the article's Creative Commons licence and your intended use is not permitted by statutory regulation or exceeds the permitted use, you will need to obtain permission directly from the copyright holder. To view a copy of this licence, visit <http://creativecommons.org/licenses/by-nc-nd/4.0/>.

© The Author(s) 2025